An Improved Empirical Wavelet Transform for Noisy and Non-Stationary Signal Processing

CUIFANG ZHUANG AND PING LIAO

School of Mechanic and Electronic Engineering, Central South University, Changsha 410006, China

Corresponding author: Cuifang Zhuang (785402842@qq.com)

ABSTRACT Empirical wavelet transform (EWT) has become an effective tool for signal processing. However, its sensitivity to noise may bring side effects on the analysis of some noisy and non-stationary signals, especially for the signal which contains the close frequency components. In this paper, an improved empirical wavelet transform is proposed. This method combines the advantages of piecewise cubic Hermite interpolating polynomial (PCHIP) and the EWT, and is named PCHIP-EWT. The main idea of the proposed method is to select useful sub-bands from the spectrum envelope. The proposed method selects the maximum points of the spectrum to reconstruct the spectrum envelope on the basis of PCHIP. Then, a new concept and a threshold named the Local Power (LP) and λ are defined. Based on the new concept LP and the λ, the useful sub-bands can be obtained. Finally, the experimental results demonstrate that the PCHIP-EWT is effective in analyzing noise and non-stationary signals, especially those that contain the closely-spaced frequencies.

INDEX TERMS Empirical wavelet transform (EWT), spectrum envelope, piecewise cubic Hermite interpolating polynomial (PCHIP), sub-bands, noisy signal.

I. INTRODUCTION

Most real systems are worked in the complex dynamic environment, while the dynamic response of these complicated mechanisms are high nonlinear, which brings many difficulties to the signal feature extraction. To analyze these types of signals, wavelet transformation (WT) is proposed. It attempts to decompose the processed signals into a set of intrinsic modes and separate the dominant or interesting features from other irrelevant modes by some criteria. This approach has been proved to be very effective for analyzing noisy and non-stationary signals. But it needs to predetermine basis functions and subdivision scheme, which significantly limits its application [1]. Therefore, how to decompose the noisy and non-stationary signals adaptively has become a focus in research. One of them is the Empirical mode decomposition (EMD) proposed by Attoh-Okine *et al.* [1]. The basic idea of the EMD is to decompose the signal into multiple Intrinsic Mode Functions(IMFs) adaptively. In [2], [3] presented that the EMD has good results for the diagnosis of heart diseases in the electrocardiogram (ECG). Edwards *et al.* [4] proved that this approach is effective for fault diagnosis in rotating machinery. However, it is generally known that the EMD suf-

fers from some drawbacks such as boundary effect and mode mixing [5]. Therefore many experts and scholars put forward some methods to improve its performance. In [6], Smith put forward an improved approach called local mean decomposition (LMD). The LMD iteration process uses local means and magnitude to decompose the data instead of the cubic spline which is used in the EMD. And the LMD has been proven to be more effective than the EMD in analyzing amplitude and frequency modulated signals. Jain and Pachori [7]proposed a new iterative approach called eigenvalue decomposition (EVD) and proved that the EVD is neither affected by the ratio of their mean frequencies nor by their relative amplitudes. Li *et al.* [8]used the order-statistics filters to replace the traditional interpolation methods of the EMD and testified that the processed method is fast, time- efficient and effective. Besides the EMD and improved EMD method, some new approaches have emerged to the signal decomposition. Dragomiretskiy and Zosso [9]put forward a new approach named variational mode decomposition (VMD). The VMD is not only effective for the noisy and non-stationary signal decomposition but also has a solid mathematical foundation which is favorable for wide application. After that, Liu *et al.* [10] came up with an improved VMD approach that combines VMD and detrended fluctuation analysis (DFA) named DFA-VMD. The noisy and non-stationary signals are first

The associate editor coordinating the review of this manuscript and approving it for publication was Lorenzo Mucchi.

broken down by the VMD and then reconstructed by the DFA. Although the DFA-VMD has the same computational complexity and time complexity with the EMD, it performs better than the EMD in denoising and discrete wavelet threshold filtering. The VMD method has a solid mathematical foundation, but it is difficult to pre-determine some parameters, which restricts its application.

Recently, Gilles [11] proposed a new method named EWT which can decompose the noisy and non-stationary signals into several IFMs adaptively. The EWT is an adaptive decomposition method which extracts narrow-band frequency components from the analyzed signal based on the frequency information contained in the signal spectrum. Compared with the EMD, the EWT performs more effectively in processing the noisy and non-stationary signals. After the EWT was introduced, it has been widely used in many fields and achieved positive results. Yu *et al.* [12]used the EWT to compound faults decoupling diagnosis of rolling bearings and proved that the mode mixing and overestimation can be resolved by EWT. Chen *et al.* [13] applied the EWT to generator bearing fault diagnosis for wind turbines and obtained good results. Kedadouche *et al.* [14] drew a comparison between the EWT and EMD in fault diagnosis field and proved that the EWT has superior performance in obtaining the frequency and associated harmonics of the faulty bearing. Zheng *et al.* [15] applied the EWT to the fault diagnosis of the rotor system with local rubbing and proved that the EWT shows a better effect than the EEMD and EMD. In [16], Cao *et al.* used the EMT in the wheel-bearing fault diagnosis of trains. However, along with the wide application in various fields, some drawbacks of EWT have already appeared, such as improper segmentations when the noisy and non-stationary signals are processed. Thus, many improved methods were proposed in order to solve the aforementioned shortcomings of the EWT. Chen *et al.* [13]used wavelet spatial neighboring coefficient denoising before applied the EWT to obtain the accurate modes from the heavy noise signal. However,the wavelet basis function and the number of components in the decomposed signal needs to be determined in advance, which limits its application. To fulfill an adaptive signal decomposition, Zheng *et al.* [15] proposed an adaptive parameterless EWT(APEWT). The APEWT includes two parts, segmented the Fourier spectrum adaptively and established the filter group. However, the APEWT has end-point effect. In order to build appropriate boundaries for creating the wavelet filter group, Juan *et al.* [17]proposed a new adaptive multiple signal classification-empirical wavelet transform (MUSIC-EWT). Although the MUSIC-EWT not only immunes to noise but also estimates the close frequencies with high accuracy, it is hard to establish the exact order of signal subspace without prior knowledge of the signal. In [18], an enhanced empirical wavelet transform for noisy and non-stationary signal processing was proposed by Yue Hu. This method uses the order statistics filter (OSF) to modify the spectrum segmentation and applies some criteria to pick out useful peaks. However, the close frequency component cannot be decomposed

successfully. In order to obtain improved TF representation of non-stationary signals, Bhattacharyya *et al.* [19]presented a new method that combines the advantages of Fourier-Bessel series expansion and EWT called FBSE-EWT. It is difficult to pre-determine some parameters when using this method. In order to obtain correct boundaries, Luo *et al.* [20]proposed a revised method called AR-EWT. The AR-EWT detects boundaries in the auto-regressive (AR) power spectrum using the Burg algorithm and can considerably suppress white noise and non-stationary factors. However, low SNR will cause false peaks in the AR power spectrum. Wang *et al.* [21]used sparsity to guide the EWT, this proposed method can extract repetitive transients caused by single and multiple bearing defects, especially when the signal is mixed with unwanted vibration components, unknown heavy noises and modulation and resonance phenomena. However, this method fails to get rational segmentations when the signal contains closely spaced frequency components.

Considering the above methods fail to decompose closely spaced frequency components in the TF plane and reducing the number of parameters that need to be determined in advance, in this work, we present an improved empirical wavelet transform named PCHIP-EWT that detects boundaries in the spectral envelope calculated by PCHIP algorithm. The experimental results show that the proposed method not only reduce the number of invalid components but also improve the ability to deal with the noise and non-stationary signal, especially when the signal involves closely frequency components.

The structure of the paper is as follows: Section 2 briefly introduces the mathematic principles of EWT and its drawbacks. Section 3 demonstrates the proposed method. Section 4 presents the experimental results and discusses the effectiveness of the PCHIP-EWT method; Section 5 concludes the paper.

II. EMPIRICAL WAVELET TRANSFORM
A. MATHEMATICAL OF THE EWT METHOD
The EWT method is proposed by Gilles [11]. The greatest advantage of this method is that it can decompose signals adaptively and its key idea is to obtain the intrinsic mode of the signal through devising a proper wavelet filter bank. The EWT method includes three important steps: (1)getting the local maximum of the spectrum; (2)segmenting the spectrum by classifying boundaries; (3)establishing a wavelet filter group. Gilles utilizes the Littlewood-Paley and Meyer wavelets to construct the filter group [22]. In the [11], the filter group is defined by the scaling function $\phi_n(\omega)$ and the experience wavelet $\psi_n(\omega)$ through the following equation:

$$\phi_n(\omega) = \begin{cases} 1 & \text{if } |\omega| \leq \omega_n - \tau_n \\ \cos\left[\frac{\pi}{2}\alpha(\frac{1}{2\tau_n}(|\omega| - \omega_n + \tau_n))\right] \\ & \text{if } \omega_n - \tau_n \leq |\omega| \leq \omega_n + \tau_n \\ 0 & \text{otherwise.} \end{cases} \tag{1}$$

$$\psi_n(\omega) = \begin{cases} 1 & if \ \omega_n + \tau_n \leq |\omega| \leq \omega_{n+1} - \tau_{n+1} \\ \cos\left[\dfrac{\pi}{2}\alpha(\dfrac{1}{2\tau_{n+1}}(|\omega| - \omega_{n+1} + \tau_{n+1}))\right] \\ \quad if \ \omega_{n+1} - \tau_{n+1} \leq |\omega| \leq \omega_{n+1} + \tau_{n+1} \\ \sin\left[\dfrac{\pi}{2}\alpha(\dfrac{1}{2\tau_n}(|\omega| - \omega_n + \tau_n))\right] \\ \quad if \ \omega_n - \tau_n \leq |\omega| \leq \omega_n + \tau_n \\ 0 & otherwise. \end{cases} \quad (2)$$

where $\alpha(y)$ is any discretionary multinomial function within certain limits [0,1], and has the follow properties:

$$\alpha(y) = \begin{cases} 0, & if \ y \leq 0 \\ and \ \alpha(y) + \alpha(1-y) = 1, & \forall y \in [0, 1] \\ 1, & if \ y \geq 1 \end{cases} \quad (3)$$

There are so many multinomial functions satisfied these features. In this paper, we use polynomial function which is first suggested by Daubechies and used by Gilles:

$$\alpha(y) = y^4(35 - 84y + 70y^2 - 20y^3) \quad (4)$$

After the homologous wavelet filter group is established by equation (1)(2), the processing signal $x(t)$ is disassembled into several frequency bands based on EWT defined as the following:

$$W_f^\varepsilon(0, t) = IFFT(x(\omega)\phi_n(\omega)) \quad (5)$$

$$W_f^\varepsilon(n, t) = IFFT(x(\omega)\psi_n(\omega)) \quad (6)$$

where the details $W_f^\varepsilon(0, t)$ and approximation $W_f^\varepsilon(n, t)$ modulus are obtained via the inner products of the signal with the wavelet filter group and $IFFT$ means the inverse Fourier transform.

B. SHORTCOMINGS OF THE EWT METHOD

The EWT method performs well when the signals have relatively well separated Fourier spectrums, which is difficult to satisfy this condition in practical application. It brings great challenges to decomposing the signal reasonably in the following cases: producing the mode mixing problem which is caused by close frequency components and obtaining more invalid components due to the high level noise.

In Fig.1, the dotted perpendicular lines represent the detected Fourier spectrum boundaries by the EWT. Area A reveals that close frequency components cannot be segmented, and area B shows that the spectrum is divided into many parts which led to too many invalid components time domain.

The EWT also has other limitations, for example, it is sensitive to noise and needs to set some parameters in advance which is difficult to determine due to the lack of prior knowledge of signals. Therefore, it is significant to investigate a rational way to improve the empirical wavelet transform.

III. PROPOSED METHODOLOGY

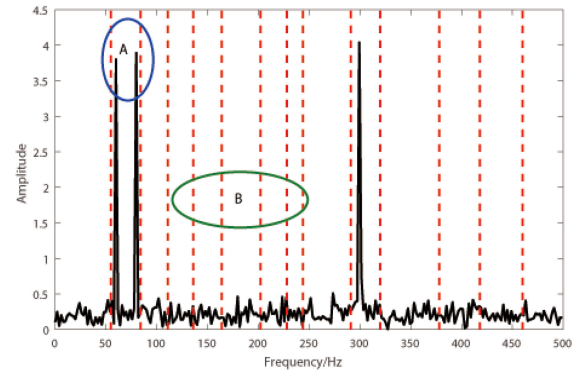In order to overcome the aforementioned drawbacks of the EWT, an improved empirical wavelet transform method

FIGURE 1. The spectrum segmentation by the EWT.

PCHIP-EWT is proposed. The PCHIP-EWT detects boundaries in the spectral envelope calculated by the PCHIP algorithm. The major steps of the PCHIP-EWT are as follows:

Step 1: Obtain the noisy and non-stationary signal $y(t)$, and acquire Fourier spectrum $Y(f)$ by the fast Fourier transform (FFT) algorithm.

Step 2: Calculate the spectrum envelope of the $K(f)$ from the spectrum $Y(f)$ based on the PCHIP. In this method, the PCHIP is able to make the Fourier spectrum $Y(f)$ more smooth. Compared to the original spectrum waveform, the spectrum envelope $K(f)$ can reduce the effects of noisy and non-stationary components to a certain extent.

Step 3: In section 3.1, calculate spectrum envelope $K(f)$ based on the PCHIP. In Section 3.2, calculate LP $p_i(f)$ of the spectrum envelope $K(f)$ and select the helpful sub-bands based on the LP and threshold λ.

Step 4: Process the signal through the EWT.

A. THE SPECTRUM ENVELOPE APPROACH BASED ON PIECEWISE CUBIC HERMITE INTERPOLATING POLYNOMIAL

The PCHIP is widely used in the global navigation satellite system to regenerate the satellite-to-earth distance from the available sparse motion data. The main reasons why the PCHIP is used to obtain the spectral envelope are explained as follows. Firstly, the PCHIP is well "shape preserving" and can not form an overshoot, so it reduces the error between the envelope and the original curve, and can truly reflect the original data [23]. Secondly, the PCHIP has good performance when processes the highly noisy and non-stationary signal [24]. Thirdly, Thirumalaisamy and Ansell [25]demonstrates that the upper spectrum envelope contains more feature information. Therefore, in this paper, obtains the upper spectrum envelope through the PCHIP. The spectrum envelope in the following paragraphs all refer to the upper spectrum envelope. We give a detailed description in the following paragraphs.

Before exploring the PCHIP in depth, we first obtain the local maximum of spectrum $Y(f)$ within the ranges [a, b]. We assume that the local maximum points and its

corresponding index are $[f_i, Y_i(f)](i = 0,1,2,\ldots,n)$, and let $Y'_i(f)$ is approximations of the derivative of $Y_i(f)$. After that we define the PCHIP function $K(f)$ as follows:

$$K(f) = \begin{cases} K_1(f), & f \in [f_0, f_1] \\ K_2(f), & f \in [f_1, f_2] \\ \ldots\ldots \\ K_n(f), & f \in [f_{n-1}, f_n] \end{cases} \quad (7)$$

where the $K_i(f), f \in [f_{i-1}, f_i]$, satisfies the following conditions:

$$K_i(f_{i-1}) = Y(f_{i-1})$$
$$K_i(f_i) = Y(f_i)$$
$$K'_i(f_{i-1}) = Y'(f_{i-1})$$
$$K'_i(f_i) = Y'(f_i) \quad (8)$$

And the $K_i(f)$ has the form:

$$K_i(f) = a_1 + a_2(f - f_i) + a_3(f - f_i)^2 + a_4(f - f_i)^2(f - f_{i+1}) \quad (9)$$

where:

$$a_1 := Y(f_{i-1})$$
$$a_2 := Y[f_{i-1}, f_i] = Y'_i(f)$$
$$a_3 := Y[f_{i-1}, f_{i-1}, f_i] = (m_i - Y'_i(f))/k_i$$
$$a_4 := Y[f_{i-1}, f_{i-1}, f_i, f_i]$$
$$= (Y'_{i+1}(f) + Y'_i(f) - 2m_i)/k_i^2 \quad (10)$$

and $\Delta Y_i(f) = Y_{i+1}(f) - Y_i(f)$, $k_i = f_{i+1} - f_i$, $m_i = \Delta f_i/k_i$.

Therefore, we can use the $K(f)$ to approximate the spectrum $Y(f)$. Here, an example to illustrate the advantages of the PCHIP is given:

$$y = \cos(2\pi x) + \eta \quad (11)$$

where η is the Gaussian white noise with 20db.

The waveform of this signal is presented in Fig.2. The red solid line represents the original signal without noise, the blue solid line is the signal mixed with noise; and the black waveform is obtained by the PCHIP. It is obvious that the black waveform is smoother than the blue one and close to the red one. Therefore, the PCHIP has the ability of noise reduction and can be used to process noise signals.

The spectrum of the signal y obtained by the FFT is shown in Fig.3(b) and the spectrum envelope based on the PCHIP is displayed in Fig.3(a). It is quite obvious that the spectrum envelope $K(f)$ is much smoother than the Fourier spectrum $Y(f)$ due to mix with less noise. In Ref [26], Adrien concludes that it is easier to decompose the signal which has a smooth spectrum. Therefore, in this paper, we use the spectrum envelope by the PCHIP instead of the Fourier spectrum to segment the boundaries.

B. PICKING OUT THE USEFUL SUB-BANDS AND DETECTING THE BOUNDARIES

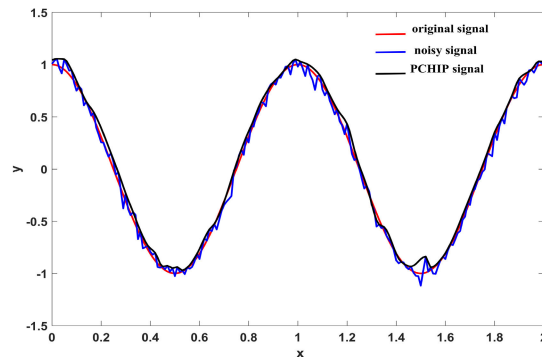After obtaining the spectrum envelope $K(f)$ based on the spectrum $Y(f)$ by the PCHIP, the helpful sub-bands are

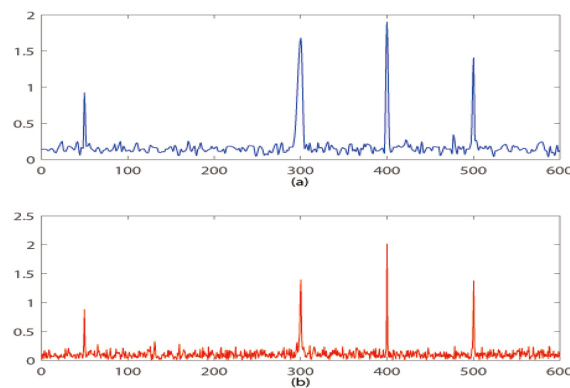**FIGURE 2.** The piecewise cubic Hermite interpolating polynomial.

FIGURE 3. (a)The spectrum envelope by the PCHIP; (b)The spectrum by the FFT.

selected. First of all, we define a new concept which is called the LP $p_i(f)$ for each sub-band as follows:

$$p_i(f) = \frac{K_{\max(i)}(f)}{f_{k_{\min(i+1)}} - f_{k_{\min(i)}}} \quad (12)$$

where $p_i(f)$ is the ith local power, $K_{\max(i)}(f)$ refers to the ith local maximum values of the $K(f)$, $f_{k_{\min(i+1)}}$ and $f_{k_{\min(i)}}$ is the index of the local minimum of the $K(f)$ which is next to the $k_{\max(i)}(f)$. Secondly, a threshold λ is defined and we can pick out the useful sub-bands by comparing the values of $p_i(f)$ and λ. If $p_i(f) \geq \lambda$, it means that this sub-band contains useful information. If $p_i(f) \leq \lambda$, it means this sub-band is consisted of noise. In such case, the most important thing is to estimate the appropriate value of the λ. Based on a large number of experiments, we conclude that the λ can be calculated by using the following equation:

$$\gamma = \frac{p_{max}}{p_{min}} \quad (13)$$

$$\lambda = \begin{cases} \dfrac{\gamma}{10} & \gamma \geq 1000 \\ \gamma & 10 \leq \gamma < 1000 \\ 10\gamma & 0 \leq \gamma < 10 \end{cases} \quad (14)$$

where p_{max} and p_{min} represent the maximum and minimum of the local power. It is worth noting that, we only present
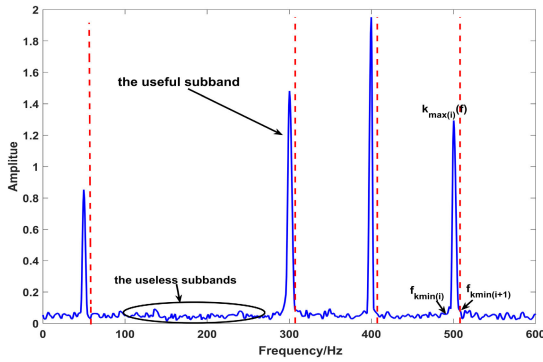
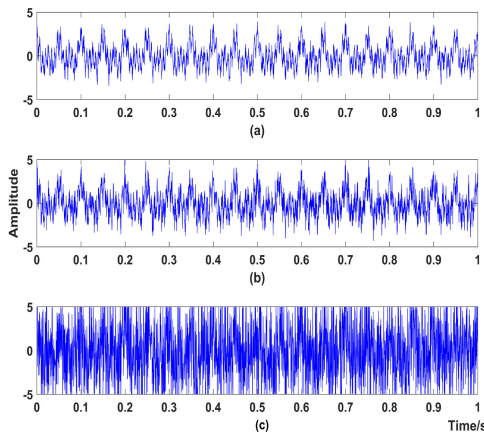**FIGURE 4.** The illustration of detecting the boundaries.

FIGURE 5. sig_1 with different SNR. (a) SNR=5db, (b) SNR=1 db, (c) SNR= −10db.

FIGURE 6. Wigner-Ville distribution of the sig_1 with different SNR. (a) SNR = 5 db, (b) SNR = 1 db, (c) SNR = −10 db.
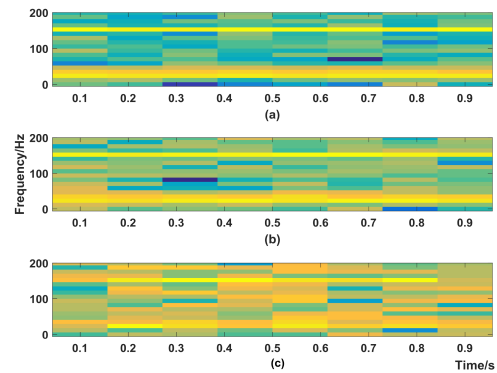
FIGURE 7. Time-frequency distribution of the sig_1 based on short-time Fourier transform with different SNR. (a) SNR=5 db, (b) SNR = 1 db, (c) SNR = − 10 db.

a simple way to calculate λ by the experiment results, but a deeper analysis is necessary to provide a more robust method.

The boundaries detection is based on the useful sub-bands obtained in the above. Each boundary is the upper cut-off frequency of the useful sub-bands in the spectrum envelope $K(f)$. If the useful sub-bands are defined as sb_n and detected boundaries are defined as w_n, then:

$$w_n = f_{k_{\min(n+1)}} \quad (15)$$

where $f_{k_{\min(n+1)}}$ is the index of the local minimum of the $K(f)$ which is the nearest to $K_{\max(i)}$ on the right. Fig.4 is given to illustrate this method. The blue line is its the spectrum envelope; the red dashed lines are the detected boundaries. The useful sub-bands and the useless sub-bands are also labeled in Fig.4.

IV. EXPERIMENTS AND RESULTS
In this section, three simulated signals and two real signals have been used to test and verify the effectiveness of the proposed PCHIP-EWT method.

A. SIMULATION EXPERIMENT
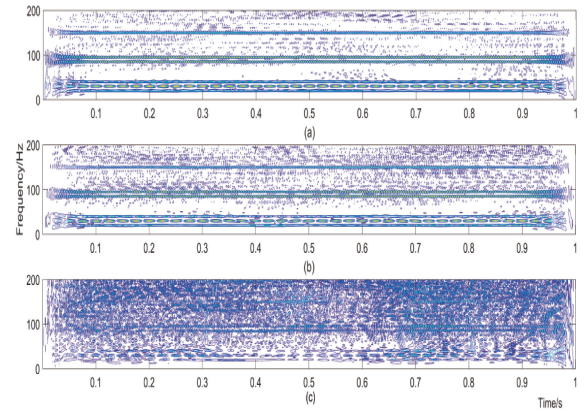*Example 1:* In example one, we have been considered a noisy signal sig_1 composed of three different frequency components(20Hz, 40Hz, and 150Hz). The frequency components of the first and second are close to each other, and the third is obviously bigger than the former. The difficulty in analyzing this signal is how to perfectly segment the signal with different levels of the white Gaussian noise. The sig_1 is defined as:
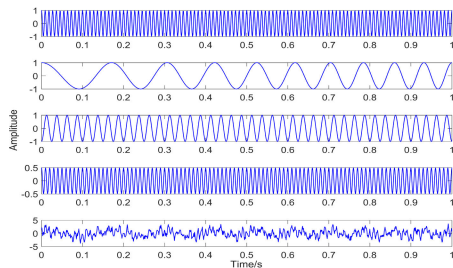
$$s_1 = \cos(40\pi t)$$
$$s_2 = cos(80\pi t)$$
$$s_3 = cos(300\pi t)$$
$$sig_1 = s_1 + s_2 + s_3 + \eta \quad (16)$$

where η is the Gaussian white noise with different signal-to-noise(SNR) (5db,1db,−10db). And different SNR means different decomposition difficulty.

Set SNR to different values(5db,1db,−10db) and the signals have been shown in Fig.5, respectively. The obtained time-frequency(TF) distribution based on the Wigner-Ville distribution and short-time Fourier transform have been presented in Fig.6 and Fig.7, respectively. It can be observed that the TF distribution becomes more obscure as the noise intensity increases. And in the Fig.6, the cross-term interference can be seen clearly, which is a major shortcoming
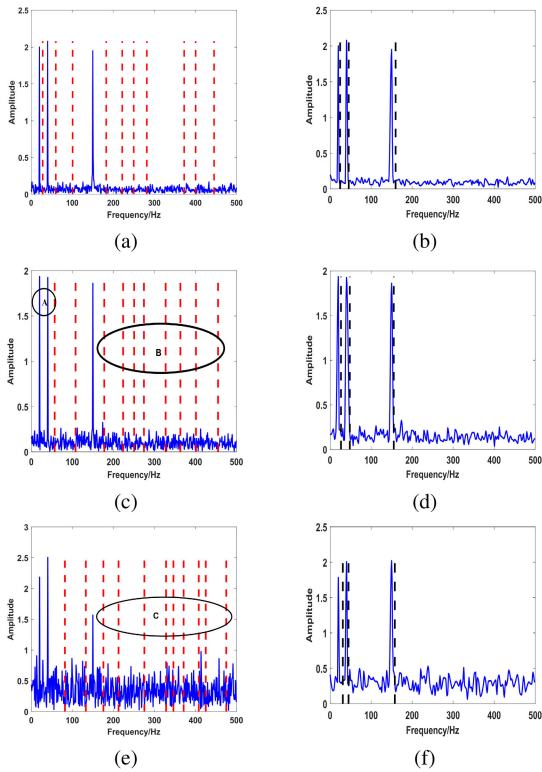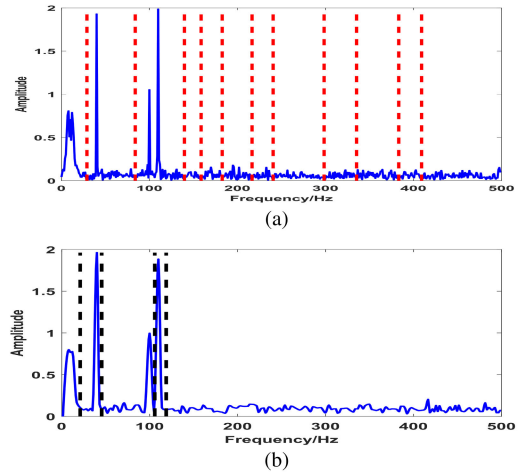
FIGURE 8. Boundaries segmented by EWT with (a) SNR = 5 db (c) SNR = 1 db, (e) SNR = − 10 db; and PCHIP-EWT (b) SNR = 5 db, (d) SNR= 1 db, (f) SNR = − 10db.
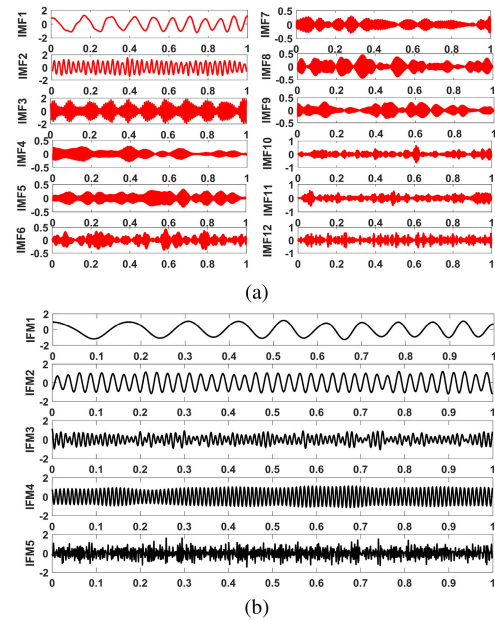

FIGURE 9. The signal sig_2 and its components.

FIGURE 10. sig_2 boundaries segmented by (a)EWT. and(b)PCHIP-EWT.

FIGURE 11. The intrinsic mode functions of (a)EWT method and (b)PCHIP-EWT method.

in Wigner-Ville distribution. The boundary segmentations by the EWT and the PCHIP-EWT have been shown in Fig.8. The comparison between Fig.8(a) and Fig.8(b) indicates that when the SNR is high (5db), both of them are able to split two components with close frequencies. But the Fig.8(a) contains more boundaries which bring more invalid components in the time domain. When the SNR is smaller (1db), the results have been shown in Fig.8(c) and Fig.8(d). The Fig.8(c) demonstrates that the EWT fails to separate close frequency components and leads to more ineffective boundaries than the Fig.8(d). In Fig.8(d), it can clearly see that the PCHIP-EWT remains effective with the reduced SNR. Compared Fig.8(e) with Fig.8(f), a similar conclusion can be obtained. Therefore, example one proves that the EWT can separate the signal whose frequencies are close when the

SNR is relatively high (5db), but is unable to separate when the signal is mixed with high noise (1db,−10db). Thus,the PCHIP-EWT provides better boundary segmentation for the sig_1 in comparison to the EWT method.

Example 2: In the example two,we have considered a more complex multi-component signal sig_2 expressed as:

$$s_1 = \cos(220\pi t)$$
$$s_2 = \cos(10\pi t + 10\pi t^2)$$
$$s_3 = \cos(80\pi t - 15\pi)$$
$$s_4 = 0.5\cos(200\pi t)$$
$$sig_2 = s_1 + s_2 + s_3 + s_4 + \eta \qquad (17)$$

where $\eta = 5\ dB$.

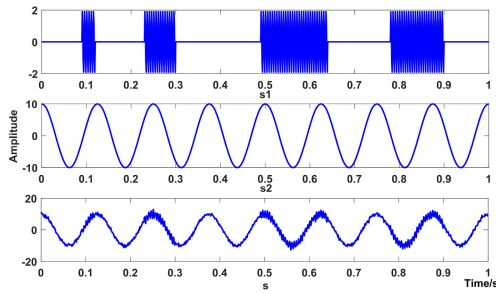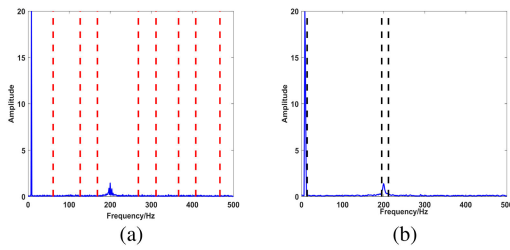**FIGURE 12.** The signal sig_3 and its components.

FIGURE 13. sig_3 boundaries segmented by (a)EWT and (b)PCHIP-EWT.

FIGURE 14. The modal components and details obtained by the EWT.(a)The components and (b)Details of (a).

FIGURE 15. The modal components and details obtained by the PCHIP-EWT.(a)The components and (b)Details of (a).

The multi-component signal has been shown in Fig.9. It can be seen that the sig_2 is composed of four components: the s_1 and the s_4 contain two close frequencies (110Hz, 100Hz) with different amplitudes, the s_2 is a chirp signal and the s_3 is a signal with constant frequency 40Hz. There are some difficulties in analyzing this signal, accurately reconstructed unstable component such as the chirp signal, segmented the signals who are consisted of close frequency components, and separated the main components from the high level white Gaussian noise.

The boundary segmentation results of both methods have been shown in Fig.10. The Fig.10(a) which the boundaries have been presented in red dotted vertical lines shows the spectrum segmentation by the EWT method and Fig.10(b) used the blue dotted vertical lines represents the spectrum segmentation by the PCHIP-EWT. Compared with the Fig.10(b), the Fig.10(a) is unable to separate the close frequency components of 100Hz and 110Hz. Meanwhile, dozens of divided domains have appeared which results in an enormous amount of ineffective components in the next step of signal decomposition. In Fig.10(b), it can be observed that the PCHIP-EWT method can generate the optimal boundaries to identify the close frequencies accurately.

The results of the sig_2 decomposition have been shown in Figs.11(a) and 11(b) for the EWT and the PCHIP-EWT, respectively. It can be seen in Figs.11(a) that IMF1 and IMF2 are the components with the frequency of 5Hz, 40Hz respectively. Apparently, there is modal aliasing in IMF3 which is consisted of two frequencies (110Hz, 100Hz) because the EWT is unable to separate the close frequencies. IMF4 and the remaining parts are ineffective components that are composed of the noise. Therefore, the EWT method
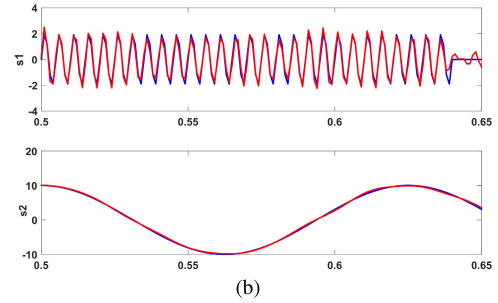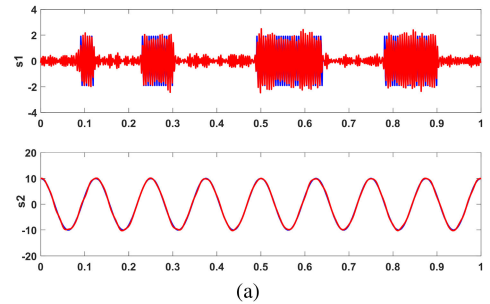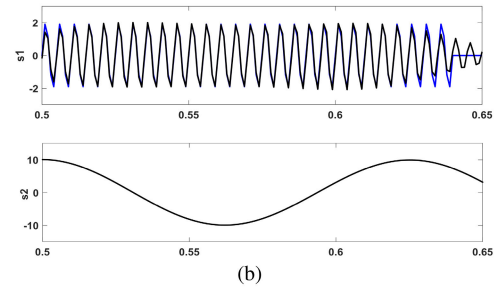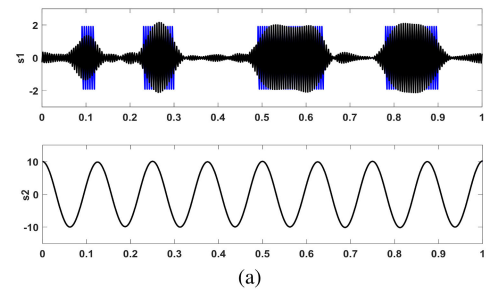
is unable to segment this multi-component signal reasonably. It is observed from the 11(b) that the four different frequencies are impeccably segregated by the PCHIP-EWT. The IMF1, IMF2, IMF3, IMF4 are the components with the frequency of 5Hz, 40Hz, 100Hz, 110Hz, and IMF5 is the noise. There are some small fluctuations in the amplitude of the spectrum on account of the noise. Taken together, this example indicates that the PCHIP-EWT more effective than the EWT method for the multi-component signal that is consisted of closed frequency components.

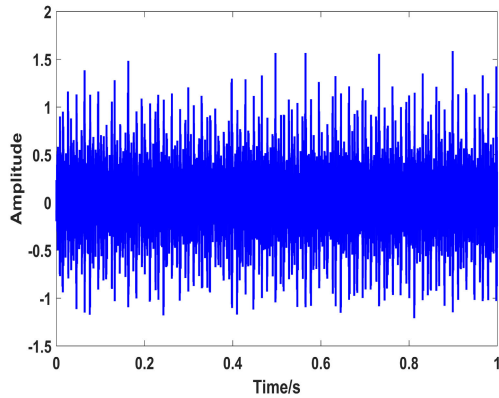| Signal	PCHIP-EWT	EWT
sig_1	0.163	0.182
sig_2	0.721	0.765
sig_3	0.295	0.854

FIGURE 16. Inner ring fault signal.

Example 3: In order to compare the performance of the PCHIP-EWT with the EWT algorithm in non-stationary synthetic signal decomposition, a signal sig_3 with high-frequency components at different times and with the White Gaussian noise has been considered:

$$s_1 = 2\sin(400\pi t)[g(t - 0.09) - g(t - 0.12)$$
$$+ g(t - 0.23) - g(t - 0.3) + g(t - 0.49)$$
$$- g(t - 0.64) + g(t - 0.78) - g(t - 0.9)]$$
$$s_2 = 10\cos(16\pi t)$$
$$sig_3 = s_1 + s_2 + \eta \tag{18}$$

where $\eta = 5db$, s_1 represents the simulation bearing fault signal and $g_{(t)}$ denotes the step signal. The signal duration is considered as 1s with a sampling rate of 1KHz.

The signal and its components have been displayed in Fig.12. The sig_3 is consisted of two different frequency components, 4Hz, and 200Hz. And the high-frequency transient component exists in four different time periods. The main challenge to analyze this signal is separated from the high-frequency transient components and the low-frequency components from the low SNR.

Detected boundaries by the EWT and the PCHIP-EWT method have been shown in Fig.13(a) and Fig.13(b), respectively. Compared these two different approaches, the EWT generates too many boundaries, which will lead to too many useless components in time decomposition. Even though there has an unnecessary boundary in Fig.13(b) due to the small amplitude of high-frequency component and the high level of noise, the PCHIP-EWT is better than the EWT.

The main components decomposed by the EWT have been shown in Fig.14(a). s_1 represents the high-frequency transient component and s_2 represents the low-frequency
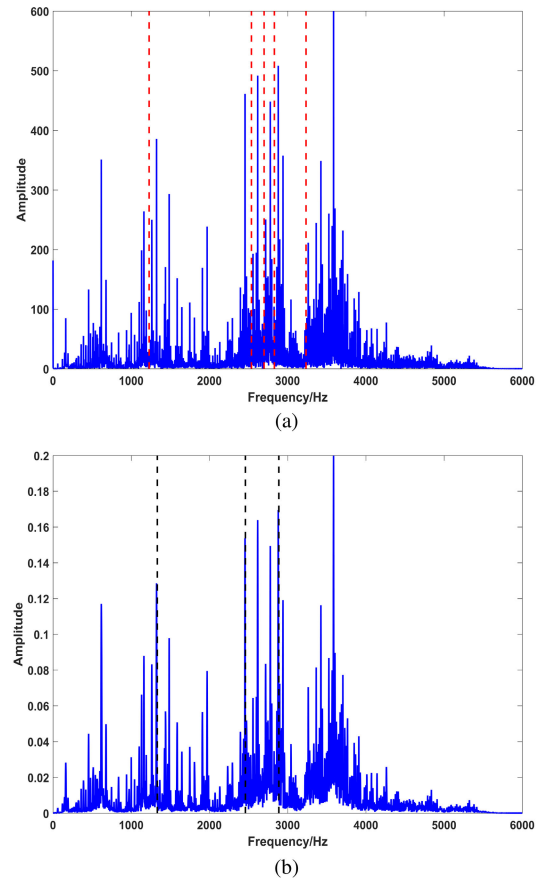

FIGURE 17. The segmentation of the boundaries (a)EWT and (b)PCHIP-EWT.
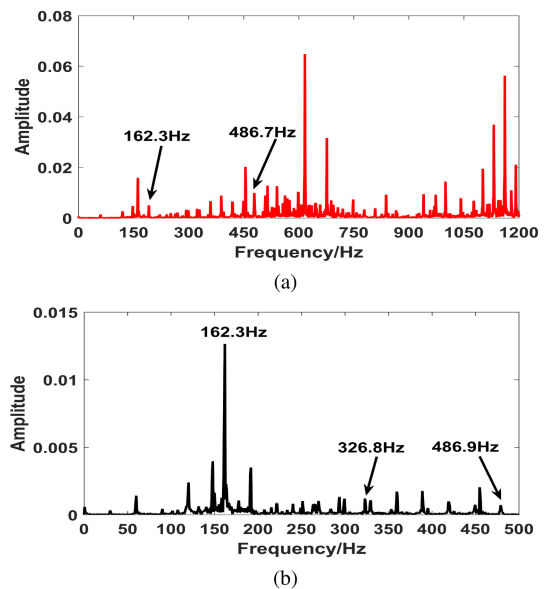

FIGURE 18. The Fourier spectrum of mode 1. (a)EWT and (b)PCHIP-EWT.

component. The detail decomposition results have been displayed in Fig.14(b). The decomposition results of the PCHIP-EWT have been shown in Fig.15(a). From the Fig.14(a)

and the Fig.15(a), we can find that there seems to be no difference between these two figures. However, the details are discrepant between the Fig.14(b) and Fig.15(b). In the high-frequency transient component, the noise-contaminated by the PCHIP-EWT is less than the EWT and s_2 which is obtained by the PCHIP-EWT is of pure low-frequency component. Therefore, the PCHIP-EWT performs well in decomposing this signal by reason of its better detected boundaries.

For evaluating reconstruction results by the PCHIP-EWT and EWT, root-mean-square-error($RMSE$) is introduced:

$$RMSE = \sqrt{\frac{1}{N}\sum_{n=1}^{N}(s(n) - \widehat{s}(n))^2} \qquad (19)$$

where $s(n)$ and $\widehat{s}(n)$ are the original signal and the reconstruction signal, respectively.

Table 1 shows the reconstruction error of PCHIP-EWT and EWT. For the sig_1 and sig_2, the reconstruction error by PCHIP-EWT is slightly less than EWT. But for the sig_3 which the signal is more complex, the performance of the PCHIP-EWT is obviously higher than EWT with the reconstruction error 0.295 and 0.854 respectively. Therefore, the proposed method is more reasonable than EWT.

B. APPLICATIONS

Example 5: The bearing fault signal used in this paper is made available publicly by Case Western Reserve University (CWRU) [27]. The bearing fault signal has a sampling rate of 12 KHz, the motor speed is 1797 RPM and the fault of the 0.007 inches in diameter is introduced at the inner raceway. Based on the rotating speed and geometrical parameters, the characteristic defect frequency of the inner race is calculated at 162Hz.

The original signal has been shown in Fig.16. There is a large number of noise in the original signal. The segmentation of the boundaries by the EWT and PCHIP-EWT have been shown in Fig.17. As is shown in Fig.17(a), The whole spectrum is divided into six regions and six different modes are obtained in total. From Fig.17(b), it can be clearly seen that the whole spectrum envelope is divided into four regions and four different modes are obtained. The Fourier spectrum of mode 1 have been shown in Fig.18(a) and (b). As is shown in Fig.18(a), the characteristic frequency of the inner race 162.3Hz and the triple failure frequency 486.7Hz obtained. In Fig.18(b), except the characteristic frequency and the triple failure frequency, the twice defect frequency 326.8Hz also can be obtained, which is an important important indicator of fault diagnosis. Meanwhile, the amplitude variation of the defect frequency and its harmonics is more suitable for fault diagnosis. Therefore, the PCHIP-EWT has better anti noise performance in bearing fault diagnosis.

Example 6: In this subsection, in order to compare the performance of the PCHIP-EWT with the EWT, the same EEG signal analyzed by Gilles [11] has been employed. The EEG signal has been shown in Fig.19. Beyond an oscillating low-frequency pattern due to the baseline wander [2] we can
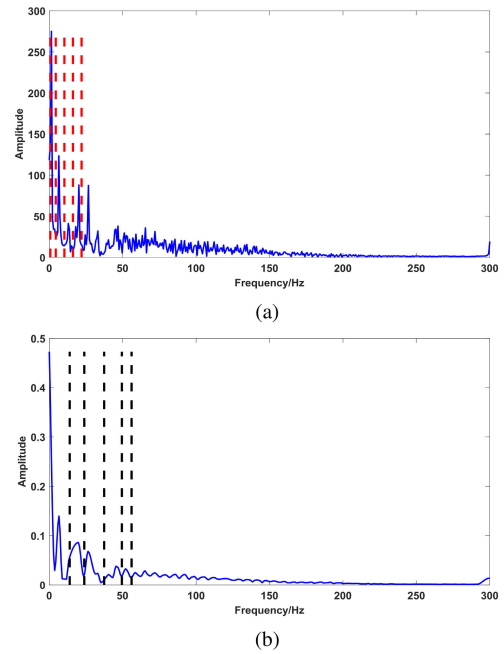
FIGURE 19. Results of the boundaries segmented on ECG signal (a)EWT and (b)PCHIP-EWT.
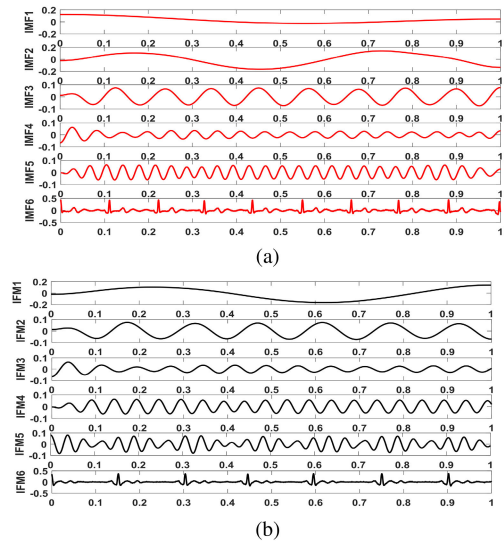
FIGURE 20. Results of the decomposition on ECG signal (a)EWT and (b)PCHIP-EWT.

clearly see the spike pulse which is driven by the rhythm [3]. Thus, the goal of analyzing this signal is to extract the helpful components from the baseline wander.

The results of the detected boundaries by the PCHIP-EWT and the EWT have been shown in Fig.20. Compared the Fig.20(a) with Fig.21(a), it can be found that the whole spectrum is divided into six regions by the EWT method and the PCHIP-EWT.The decomposition results of both methods have been displayed in Fig.21. From the Fig.21(a), it can be observed that the low-frequency is wrongly divided into two modes. Thus, the EWT fails to separate the baseline wander interference from the clean ECG signal. In Fig.21(b), it can
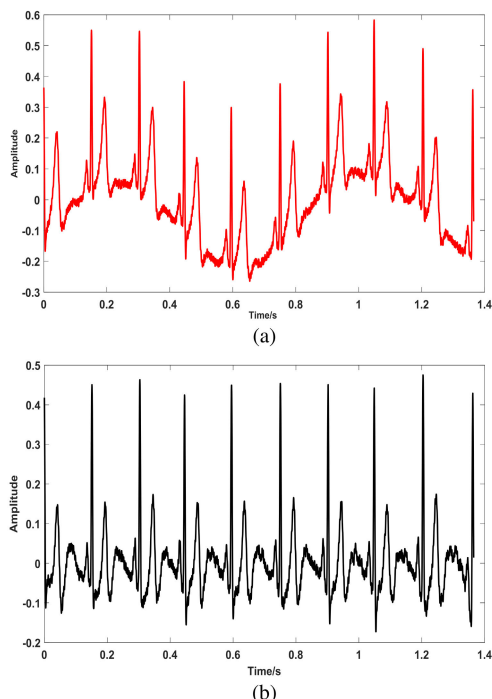
FIGURE 21. Results of the reconstruction on ECG signal (a)EWT and (b)PCHIP-EWT.
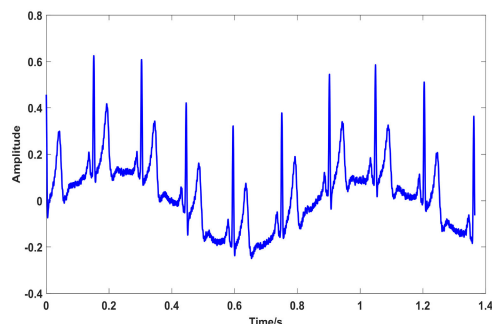

FIGURE 22. ECG signal.

be found that more rational mode decomposition result is obtained using the PCHIP-EWT algorithm. The first mode captures the low-frequency oscillation of the baseline. The second,third,four,five modes oscillates precisely at the frequency of the heartbeat; the last mode is the most prominent feature of ECG signal, named QRS complex. In [18], Hu *et al.* proves that in order to get a clean ECG signal without the baseline wander interference, the first mode should be removed. According to this theory, the reconstruction results by the PCHIP-EWT and the EWT have been shown in Fig.22. It can be found that the baseline wander interference can be removed by the PCHIP-EWT while the EWT can not. Thus, the PCHIP-EWT has a better performance than the EWT in analyzing the ECG signal.

V. CONCLUSION

In this paper, a new method called the PCHIP-EWT was proposed for the decomposition of the noisy and non-stationary signals. The Fourier spectrum was replaced by the spectrum envelope for the computation of optimal boundary detected. Three numerical simulations and two real-life example were presented for the purpose of comparing the PCHIP-EWT with the original EWT. The simulation experiment results prove that the PCHIP-EWT can successfully separate the two components, which are close to each other in the spectrum, but EWT cannot. The applications prove that the PCHIP-EWT is more suitable than the EWT in bearing fault diagnosis and EEG signal analyzes.

If the proposed method is unable to decompose the signal which includes components overlapping in both time and frequency domains such as two linear frequency modulation (LFM) chirp signals. Such cases may be addressed by building more redundancy adaptive frames. However,the PCHIP-EWT method has a good performance in analyzing many real-life noisy and non-stationary signals such as vibration signal, ECG signal and railway axle bearings fault signal. Thus the PCHIP-EWT method has potential to analyse wide classes of real life noisy and non-stationary signals.

REFERENCES

[1] N. Attoh-Okine, K. Barner, D. Bentil, and R. Zhang, "The empirical mode decomposition and the Hilbert-Huang transform," *EURASIP J. Adv. Signal Process.*, vol. 2008, no. 1, 1996, Art. no. 251518.

[2] M. Blanco-Velasco, B. Weng, and K. E. Barner, "ECG signal denoising and baseline wander correction based on the empirical mode decomposition," *Comput. Biol. Med.*, vol. 38, no. 1, pp. 1–13, Jan. 2008.

[3] S. Pal and M. Mitra, "Empirical mode decomposition based ECG enhancement and QRS detection," *Comput. Biol. Med.*, vol. 42, no. 1, pp. 83–92, Jan. 2012.

[4] S. Edwards, A. W. Lees, and M. I. Friswell, "Fault diagnosis of rotating machinery," *Meas. Instrum.*, vol. 30, no. 1, pp. 4–13, 1999.

[5] Z. Wu and N. E. Huang, "Ensemble empirical mode decomposition: A noise-assisted data analysis method," *Adv. Adapt. Data Anal.*, vol. 1, no. 1, pp. 1–41, Jan. 2009.

[6] J. S. Smith, "The local mean decomposition and its application to EEG perception data," *J. Roy. Soc. Interface*, vol. 2, no. 5, pp. 443–454, Dec. 2005.

[7] P. Jain and R. B. Pachori, "An iterative approach for decomposition of multi-component non-stationary signals based on eigenvalue decomposition of the Hankel matrix," *J. Franklin Inst.*, vol. 352, no. 10, pp. 4017–4044, Oct. 2015.

[8] H. Li, Y. Hu, F. Li, and G. Meng, "Succinct and fast empirical mode decomposition," *Mech. Syst. Signal Process.*, vol. 85, pp. 879–895, Feb. 2017.

[9] K. Dragomiretskiy and D. Zosso, "Variational mode decomposition," *IEEE Trans. Signal Process.*, vol. 62, no. 3, pp. 531–544, Feb. 2014.

[10] Y. Liu, G. Yang, M. Li, and H. Yin, "Variational mode decomposition denoising combined the detrended fluctuation analysis," *Signal Process.*, vol. 125, pp. 349–364, Aug. 2016.

[11] J. Gilles, "Empirical wavelet transform," *IEEE Trans. Signal Process.*, vol. 61, no. 16, pp. 3999–4010, Aug. 2013.

[12] J. Yu, Z. Hua, and Z. Li, "A new compound faults detection method for rolling bearings based on empirical wavelet transform and chaotic oscillator," *Chaos, Solitons Fractals*, vol. 89, pp. 8–19, Aug. 2016.

[13] J. Chen, J. Pan, Z. Li, Y. Zi, and X. Chen, "Generator bearing fault diagnosis for wind turbine via empirical wavelet transform using measured vibration signals," *Renew. Energy*, vol. 89, pp. 80–92, Apr. 2016.

[14] M. Kedadouche, M. Thomas, and A. Tahan, "A comparative study between Empirical Wavelet Transforms and Empirical Mode Decomposition Methods: Application to bearing defect diagnosis," *Mech. Syst. Signal Process.*, vol. 81, pp. 88–107, Dec. 2016.

[15] J. Zheng, H. Pan, S. Yang, and J. Cheng, "Adaptive parameterless empirical wavelet transform based time-frequency analysis method and its application to rotor rubbing fault diagnosis," *Signal Process.*, vol. 130, pp. 305–314, Jan. 2017.

[16] H. Cao, F. Fan, K. Zhou, and Z. He, "Wheel-bearing fault diagnosis of trains using empirical wavelet transform," *Measurement*, vol. 82, pp. 439–449, Mar. 2016.

[17] J. P. Amezquita-Sanchez and H. Adeli, "A new music-empirical wavelet transform methodology for time–frequency analysis of noisy nonlinear and non-stationary signals," *Digit. Signal Process.*, vol. 45, pp. 55–68, 2015.

[18] Y. Hu, F. Li, H. Li, and C. Liu, "An enhanced empirical wavelet transform for noisy and non-stationary signal processing," *Digit. Signal Process.*, vol. 60, pp. 220–229, Jan. 2017.

[19] A. Bhattacharyya, L. Singh, and R. B. Pachori, "Fourier–Bessel series expansion based empirical wavelet transform for analysis of non-stationary signals," *Digit. Signal Process.*, vol. 78, pp. 185–196, Jul. 2018.

[20] Z. Luo, T. Liu, S. Yan, and M. Qian, "Revised empirical wavelet transform based on auto-regressive power spectrum and its application to the mode decomposition of deployable structure," *J. Sound Vib.*, vol. 431, pp. 70–87, Sep. 2018.

[21] D. Wang, Y. Zhao, C. Yi, K.-L. Tsui, and J. Lin, "Sparsity guided empirical wavelet transform for fault diagnosis of rolling element bearings," *Mech. Syst. Signal Process.*, vol. 101, pp. 292–308, Feb. 2018.

[22] I. Daubechies and C. Heil, "Ten lectures on wavelets," *Comput. Phys.*, vol. 6, no. 6, p. 697, 1992.

[23] S. Lu, Y. Wang, and Y. Wu, "Novel high-precision simulation technology for high-dynamics signal simulators based on piecewise hermite cubic interpolation," *IEEE Trans. Aerosp. Electron. Syst.*, vol. 54, no. 5, pp. 2304–2317, Oct. 2018.

[24] L. Shulin, Z. Haifeng, W. Hui, and M. Rui, "Application of improved EMD algorithm for the fault diagnosis of reciprocating pump valves with spring failure," in *Proc. 9th Int. Symp. Signal Process. Appl.*, Feb. 2007, pp. 1–4.

[25] M. R. Thirumalaisamy and P. J. Ansell, "Fast and adaptive empirical mode decomposition for multidimensional, multivariate signals," *IEEE Signal Process. Lett.*, vol. 25, no. 10, pp. 1550–1554, Oct. 2018.

[26] A. Deliège and S. Nicolay, "Extracting oscillating components from nonstationary time series: A wavelet-induced method," *Phys. Rev. E, Stat. Phys. Plasmas Fluids Relat. Interdiscip. Top.*, vol. 96, no. 3, 2017, Art. no. 033307.

[27] A. Boudiaf, A. Moussaoui, A. Dahane, and I. Atoui, "A comparative study of various methods of bearing faults diagnosis using the case Western Reserve University data," *J. Failure Anal. Prevention*, vol. 16, no. 2, pp. 271–284, Apr. 2016.

CUIFANG ZHUANG was born in Hubei, China. She received the B.S. degree from the School of Electronic Information, College of Science and Arts, Jianghan University, Hubei, in 2013, and the M.S. degree from the Institute of Physical Information, Hunan Normal University, Hunan, China, in 2016. She is currently pursuing the Ph.D. degree in mechanic and electronic engineering with Central South University, Hunan. Her research interests are in remaining useful life prediction of the rotor.

PING LIAO received the B.S. degree from Northwestern Polytechnical University, Xi'an, China, in 1986, the M.S. degree from the Nanjing University of Aeronautics and Astronautics, Nanjing, China, in 1993, and the Ph.D. degree from Central South University, Hunan, China, in 2003. He is currently a Professor of mechanic and electronic engineering with Central South University. His research interests include intelligent diagnostics for plant machinery and signal processing.

• • •